



Periodicity test for LSI +61°303

N. Sidro, J. Rico, J. Cortina (IFAE)

November 14th, 2007

Abstract

Here we report on the periodicity of the very high energy γ -ray emission from the radio emitting X-ray binary LSI +61°303 detected also by MAGIC. The data have been taken in two campaigns along 10 different orbital periods. The high energy emission has been found to be variable, and the fact that the detections occur at similar orbital phases, suggests that the emission is periodic.

To test for possible periodic structures in the light-curve, we use the formalism developed by Lomb and Scargle [1, 2] and the Rayleigh statistic test [3]. We apply both methods to the LSI +61°303 data taken in cycle I and II separately as well as to its combination (referred to as I+II).

With merging both campaigns we found the LSI +61°303 data set to be periodic with a post-trial probability of 10^{-9} , with a period value of 26.78 ± 0.09 days. The frequency error has been estimated as a propagation of the Poissonian measurement errors without any signal shape assumption.

Contents

1	Introduction	2
2	Data description	2
3	Statistical tests	2
3.1	Rayleigh test	4
3.2	Lomb-Scargle test	4
3.3	Natural frequencies	5
3.4	Chance probability	7
3.4.1	Pre-trial probability	8
3.4.2	Post-trial probability	9
4	Technical considerations	12
4.1	Unphysical peaks in the periodogram	12
4.2	Merging data form different observational campaigns	15
5	Results	17
5.1	Periodograms over LSI +61°303 data	17
5.2	Analysis for different time bins	22
5.3	Peak frequency and error estimation	24
6	Conclusions	25

1 Introduction

LSI +61°303 is a binary system located at 2 kpc from us, composed of a compact object of unknown nature (neutron star or black hole) in a highly eccentric ($e = 0.7$) orbit around a bright ($V \sim 10.8$) Be star. The system presents strong, periodic radio outbursts [4], associated to the orbital period of the binary system: 26.496 days. The periastron passage is at phase $\phi = 0.23 \pm 0.02$ [5]. The phase and intensity of the radio outburst show a modulation of 4.6 years [6].

Optical [7] and X-ray [8] observations detected a variable emission at timescales similar to the radio ones. The detected periodicity at those different energy ranges is also associated to the orbital modulation. LSI +61°303 was first observed in γ -rays by the COS-B experiment and later EGRET measurements showed hints of variability of the γ -ray flux [9], although no periodicity is proven with those measurements. The aim of this work is to search for periodicity in the LSI +61°303 TeV data.

In the next sections we describe the methods used for analysing the temporal characteristics of LSI +61°303 MAGIC data. The aim of this study is to find whether within the LSI +61°303 TeV observations exists a periodic behaviour. The data consists of a series of γ -ray candidates arrival times which may be folded at a given frequency to produce a phase distribution of the total data set. Periodicity may be more easily detected in the phase distribution than in sparse data.

In order to test for possible periodic structures in the TeV light-curve, we will use two methods: the formalism developed by Lomb and Scargle [1, 2] and the Rayleigh statistic test [3]. We first present the TeV data sample. Then we will review the statistical tests and describe the methods used for obtaining the chance probability. Then we will apply them to the TeV LSI +61°303 data.

2 Data description

The observations were performed in two campaigns. In the **first campaign** LSI +61°303 was observed for 54 h (after standard quality selection, discarding bad weather data) between October 2005 and March 2006, covering six orbital periods. About 22 % of the data were recorded under moonlight conditions. The **second campaign** lasts from September to December 2006. This observation covered 4 orbital periods, and a total amount of 112 h (after quality selection) were recorded, 17% of which were taken under moon light conditions. While in campaign I the observations were carried out in ON/OFF mode, in campaign II the data were taken in wobble mode [10], i.e. by alternately tracking two positions at 0.4° offset from the camera center. The covered zenith angle range in both campaigns is between 32 - 55° .

The measurements from both campaigns show that the VHE γ -ray emission from LSI +61°303 is variable. The γ -ray flux above 400 GeV as a function of phase is shown in Fig. 1. The flux has a maximum corresponding to about 16% of the Crab nebula flux, and is detected at around phase 0.6. A later maximum is also seen in the last observed period at phase ~ 0.84 . The probability for the distribution of measured fluxes to be a statistical fluctuation of a constant flux (obtained from a χ^2 fit of a constant function to the entire data sample) is 3×10^{-5} and 3×10^{-13} for each campaign respectively. The fact that the detections occur at similar orbital phases already hints at a periodic nature of the VHE γ -ray emission.

3 Statistical tests

When a periodic signal with a certain frequency and/or shape is expected, a specific test for that case can be applied; otherwise a more general test of uniformity must be used. Two of the basic tests of the latter class are the Rayleigh [3] and the Lomb-Scargle tests [2]. Both are based on the Fourier transform, which we introduce here.

A physical variable x_j (the number of γ -ray event candidates in our case) is measured a set of times t_j where

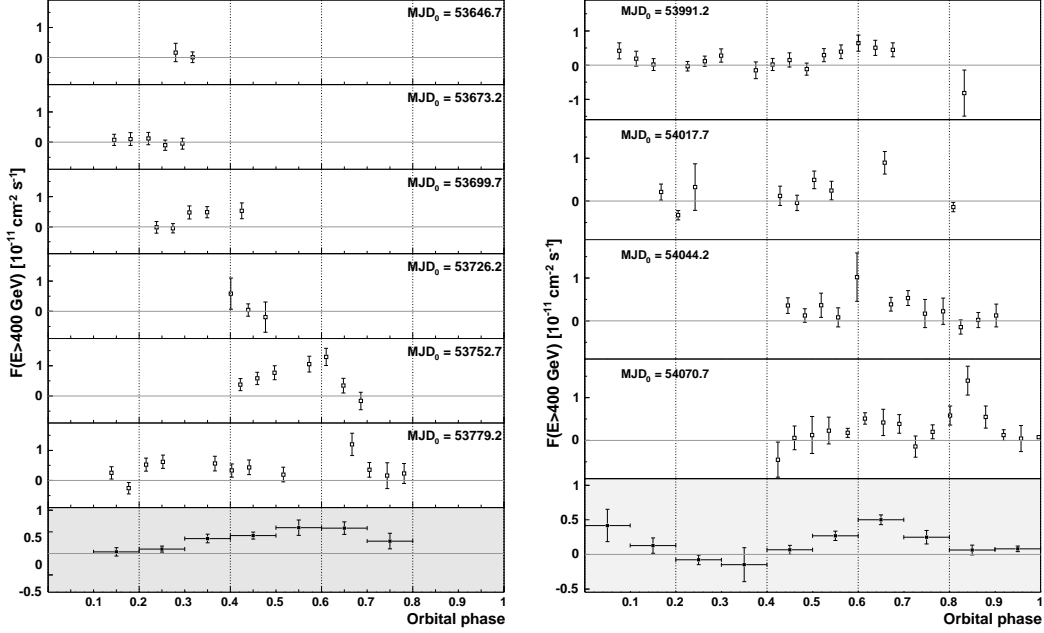


Figure 1: VHE γ -ray flux of LSI +61°303 as a function of orbital phase, for the first (left panel) and second (right panel) campaign observations. In the upper panels, the six and four observed orbital periods are shown, with one point per observation night. Bottom grey panels show the averaged flux for each observation campaign. Vertical error bars include 1σ statistical error and 10% systematic uncertainty on day-to-day relative fluxes. The modified Julian date (MJD) corresponding to orbital phase 0 is indicated for every orbital period.

$j = 1, \dots, n$. The discrete Fourier transform is defined as

$$FT_X(\omega) = \sum_{j=1}^n x_j e^{-i\omega t_j} \quad (1)$$

where ω is the angular frequency. The so-called classical periodogram (spectral power as a function of frequency) is defined as:

$$\begin{aligned} P_{\text{class}}(\omega) &= \frac{1}{n} |FT_X(\omega)|^2 \\ &= \frac{1}{n} \left[\left(\sum_{i=1}^n x_i \cos(\omega t_i) \right)^2 + \left(\sum_{i=1}^n x_i \sin(\omega t_i) \right)^2 \right] \end{aligned} \quad (2)$$

([2] and references therein). If the measured signal is dominated by a sinusoidal component with angular frequency ω_0 , the factors x_j and $e^{-i\omega_0 t_j}$ are in phase. As a result, the sums in Eq. 2 and therefore the periodogram $P_{\text{class}}(\omega)$ reaches a local maximum for ω equal or close to ω_0 . At frequencies significantly different from ω_0 the factors x_j and the exponential are out of phase, the individual factors of the sum cancel with each other in average and the periodogram has a small value. Thus, prominent frequency components in the data are visible as peaks in the periodogram.

In the case of *even data spacing*, the significance of a certain frequency component is estimated by means of hypothesis testing: Given the null hypothesis that the data sample only consists of Gaussian white noise¹, the periodogram has an exponential probability density function (PDF):

$$\mathcal{P}(z < P_{\text{class}}(\omega) < z + dz) = e^{-z} dz \quad (3)$$

We treat in detail the problem of the significance estimation in Section 3.4.

3.1 Rayleigh test

The Rayleigh power at a particular frequency is a measure of the probability that the data contain a sinusoidal component pulsed at that frequency. It is an hypothesis test, used to ascertain whether or not a signal is present in a data set. It is a special case of the classical periodogram, where t_i for $i = 1, \dots, n$ are the set of arrival times where γ -ray event candidates are detected (also called *sampling*).

We search for a sinusoidal signal in the data at the angular frequency $\omega = 2\pi\nu$. The power of the Rayleigh test $R(\omega)$ as a function of the angular frequency ω (the periodogram) is given by:

$$R(\omega) = 2n \left[\left(\frac{1}{n} \sum_{i=1}^n \cos(\omega t_i) \right)^2 + \left(\frac{1}{n} \sum_{i=1}^n \sin(\omega t_i) \right)^2 \right] \quad (4)$$

In absence of a periodic signal, $R(\omega)$ is distributed as a χ^2 with two degrees of freedom as n tends to infinity. This is so because $\cos \omega t_i$ and $\sin \omega t_i$ are Gaussian distributed, the square of a Gaussian variable is χ^2 distributed and the sum of χ^2 variables is also a χ^2 variable for which the number of degrees of freedom is given by the sum of the degrees of freedom from the individual variables. In general, the χ^2 PDF with k degrees of freedom is

$$PDF(\chi^2) = \frac{(1/2)^{k/2}}{\Gamma(k/2)} x^{k/2-1} e^{-x/2} \quad (5)$$

Then the χ^2 for $k = 2$ degrees of freedom is an exponential function (recovering the result of Eq. 3).

But this exponential behaviour is only achieved for uniform random distributions, where the arrival times t_i are homogeneously sampled over time or *evenly sampled*. If the set of arrival times is *unevenly sampled* (arbitrary t_i 's) or has gaps with uncovered phases, Eq. 5 does not hold and a dedicated Monte Carlo must be developed to determine the PDF of the Rayleigh power. We develop further on this issue in Section 3.4.

In the case of LSI +61°303 TeV data, we perform the test using as physical quantities t_i , the arrival times of the events passing all signal selection cuts (including θ^2 cut). These events are referred to as the ON sample. Note from Eq. 4 that the t_i are the only measured quantities entering the Rayleigh test. For the sake of computing the chance probability (see Sec. 3.4) we merge the events into 15 minute bins, and assign all of them a common, average arrival time. This has no practical effect on the accuracy of the periodogram since the scanned frequencies are much smaller than $\frac{1}{15\text{min}} = 96 \text{ day}^{-1}$. We discuss about the effect of selecting different binnings in Section 5.2.

3.2 Lomb-Scargle test

In the case of *unevenly sampled* data, one can recover a relatively simple behaviour of the power PDF with a slightly modified definition of the classical periodogram. The Lomb-Scargle periodogram as a function of the angular frequency ω is defined as [2]:

$$P(\omega) = \frac{1}{2\sigma_X^2} \left[\frac{[\sum_{i=1}^n (x_i - \bar{X}) \cos(\omega(t_i - \tau))]^2}{\sum_{i=1}^n \cos^2(\omega(t_i - \tau))} + \frac{[\sum_{i=1}^n (x_i - \bar{X}) \sin(\omega(t_i - \tau))]^2}{\sum_{i=1}^n \sin^2(\omega(t_i - \tau))} \right] \quad (6)$$

¹A time series of independent Gaussian random numbers is denoted as Gaussian white noise

with the phase factor τ given by the equation:

$$\tau = \frac{1}{2\omega} \arctan \left(\frac{\sum_{i=1}^n \sin(2\omega t_i)}{\sum_{i=1}^n \cos(2\omega t_i)} \right) \quad (7)$$

and \bar{X} and σ_X^2 the mean and variance of the variable x_i . The constant τ is a kind of offset that makes $P(\omega)$ completely independent of shifting all the t_i 's by any constant.

The Lomb-Scargle periodogram has the same theoretical exponential PDF as the classical periodogram (in case of evenly spaced data, expression 6 tends to 2). This statement, however, relies on the fact that the periodogram is normalised onto the variance σ_X^2 . When the variance is not known a priori, it has to be estimated from the data themselves. As a result the PDF (Eq. 3) changes into [11]:

$$\mathcal{P}(z < P(\omega) < z + dz) = \left(1 - \frac{2z}{n}\right)^{\frac{n}{2}} dz \quad (8)$$

For small Fourier power values z and a large number of data points n , this distribution converges to the exponential distribution.

In the case of LSI +61°303 TeV data, the variable used in the test, x_i , is the number of arrival γ -ray candidates in a time interval $[t_i - \frac{\Delta t}{2}, t_i + \frac{\Delta t}{2}]$ (where Δt is the time binning) passing all signal selection cuts and background subtracted (so called N_{ex}), which can be positive (excess) or negative (defect). As in the Rayleigh test, and for the sake of computing the chance probability (see Sec. 3.4) we merge the events into 15 minute bins, and assign all of them a common, average arrival time.

3.3 Natural frequencies

Given n data points there is a discrete finite set of $n/2$ independent frequencies in the periodogram. For the case of *evenly spaced* data there is a natural set of frequencies

$$\omega_k = 2\pi k/T; \quad k = 1, \dots, n/2 \quad (9)$$

where $T = t_{last} - t_{first}$ is the total time interval spanned by the data set. These frequencies are selected so that their discrete Fourier transform (Eq. 1) contains just enough information to recover the original data. The Fourier power values $FT(\omega_k)$ are independent of each other.

The fundamental frequency $\omega_1 = 2\pi/T$, corresponds to a sine wave of period equal to the whole interval T and is the lowest frequency for which the data contain relevant information.

The so-called Nyquist frequency is $\omega_{Ny} = \omega_{n/2} = \pi n/T = \pi \Delta t$ where $\Delta t = T/n$ is the sampling interval. This characterises the largest frequency component which can be resolved by the given data spacing Δt . In table 1 we show the value of the fundamental and Nyquist frequencies for the studied data samples.

Campaign	n points	T (days)	ν_1 (IFS) (d^{-1})	ν_{Ny} (d^{-1})
I	211	145	0.00686	0.723
II	491	103	0.00972	2.386
I+II	702	441	0.00226	0.794

Table 1: For each observational campaign we show the number of points (using 15 minute bins), the total elapsed time T and the fundamental (or Independent Fourier Spacing) and Nyquist frequencies.

In case the sampling is *uneven*, the situation becomes more complex, since the independence among the natural frequencies is lost. But if the frequency grid is well chosen, the degree of dependence between the powers at the different frequencies is usually small.

The fundamental frequency ω_1 is unchanged for even or uneven sampling, since the interval T is still well defined. But the Nyquist frequency might change with the data sampling (especially when the data points are closely clumped together, like in our case). The Nyquist frequency can be estimated by means of the *spectral* or *periodogram window* [2]:

$$W(\omega) = \frac{1}{N} \left| \sum_{j=1}^n e^{-i\omega t_j} \right|^2 \quad (10)$$

This function evaluated at $W(\omega - \omega')$ gives the correlation coefficient between $P(\omega)$ and $P(\omega')$ for arbitrary ω and ω' . Thus this quantity contains all relevant information about dependencies and correlations. For independence of $P(\omega)$ and $P(\omega')$, it is necessary (but not sufficient) that $W(\omega - \omega') = 0$. Furthermore, for mutual independence of a set $P(\omega_k)$ of spectral powers, it would be also necessary (but not sufficient) to have the ω_k evenly spaced. These are very difficult conditions to realise in practice.

The power of the final periodogram is actually given by the convolution of the true physical process with the spectral window. The pathology of the data distribution is all contained in the spectral window, which can be calculated from the data spacing alone, and does not depend directly on the data themselves. The interference of the spectral window can be described as one of two types: due to the finite length of the data and due to the data spacing, which is called *aliasing*. For continuously recorded data, aliasing does not exist, while for equally spaced data, it exists in its most extreme form. In astronomical observations, such aliasings often arise due to a one day, one month, or one year gaps in the data.

The straightforward generalisation of the windowing function to the Lomb-Scargle periodogram (replacing the term $x_i - \bar{X}$ in Eq. 6 by unity) is not completely correct window function ([2], Appendix D), but nevertheless gives some hints on the independent frequency components. The periodogram window in the LSI +61°303 TeV data in the second campaign is shown in Fig. 2. The maximum shows up at $\nu = 1\text{d}^{-1}$ (day-night interruptions). In campaign II the step between the natural frequencies is $\nu_1 = \frac{1}{103\text{days}} \simeq 0.01\text{d}^{-1}$ for which the windowing function is $W(0.01) \simeq 10$. This means that there is correlation between the scanned frequencies.

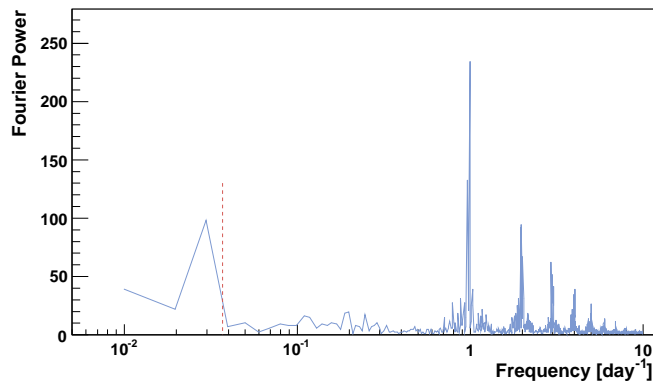


Figure 2: Windowing function as derived for the LSI +61°303 data in campaign II. The red dotted line marks the LSI +61°303 orbital period of 26.496 days.

But in spite of the loss of independence of the random variables $P(\omega)$ at the natural frequencies, the *chance probability* (see below Sec. 3.4) still provides a reliable significance test [12]. We will evaluate the modified periodogram at the natural frequencies defined by the data span, and use the chance probability calculated or estimated from the Monte-Carlo simulation (see Sec. 3.4) for unevenly spaced data to evaluate the significance of the periodogram peaks.

In this study, we scan frequencies up to 0.25 d^{-1} , which covers the frequency of interest ($1/26.496 = 0.038 \text{ d}^{-1}$) while keeping relatively low the number of trials.

3.4 Chance probability

Given the probability distribution for the spectral power, we can write down an expression for the so called *post-trial chance* or *false alarm* probability. If the probability that a spectral power z is above some value z_0 is $\mathcal{P}(z > z_0)$ (also called *pre-trial* probability), then the post-trial probability is

$$F = 1 - [1 - \mathcal{P}(z > z_0)]^M \quad (11)$$

where M is the number of independent frequencies that were examined. Thus F is the probability that *at least one* of the computed powers z is above the threshold z_0 . A small value for the chance probability indicates a highly significant periodic signal.

However the principal difficulty encountered when searching for a false alarm function in the case on unevenly spaced data is the loss of the independence of the natural frequencies (see Section 3.3). The only alternative to a theoretical chance probability function is an empirically generated one.

The practical method for determining the chance probabilities is, as suggested by [12], the following:

1. Using the sampling times of the actual data set to be analysed, we construct a large number of random data series.
2. Select a convenient grid of frequencies that cover the frequency range in the periodogram that is to be inspected (see Section 3.3 for how to choose them).
3. For each random series, we construct a periodogram sampling it for the selected frequencies.
4. For each frequency, we compare the power of the real data set with the PDF obtained from the random series, in order to determine empirically the (pre-trial) probability of this power to happen by chance.
5. The overall (post-trial) chance probability is computed by the following generalisation: for each simulated data series we inspect the corresponding periodogram, identify the highest power that occurs at **any** of the pre-selected frequencies, and use its highest values to construct the post-trial PDF.

Integration of the PDF from a given power value z_0 we obtain an empirical cumulative probability function (CPF) which is used to determine the probability that pure noise alone could produce a power higher than or equal to a given threshold power value z_0 for one (pre-trial) or any (post-trial) of the selected frequencies, where the influence of the uneven sampling in the observation time has been removed.

The maximum achieved power in the CPF constructed in this way depends on the number of generated random data series. If a power obtained with the data series to be studied is under the maximum power in the CPF, we empirically determine the probability. If on the contrary, we get a power above the maximum, we can fit the CPF with the false alarm function of choice. If a sufficiently good fit is obtained, the fitted function can be used to calculate the significance levels for the given data set.

If the fit is not good however, the significance levels predicted by these fitted functions are likely to lead to erroneous rejection or acceptance of periodogram peaks, making them almost useless in the assessment of the significance peaks. In such cases, we can only use the empirical CPF to give a limit on the probability for a given data set, up to the level of the maximum obtained power in the CPF.

We apply this method to the LSI $+61^\circ 303$ data sample in order to obtain the pre and post-trial probabilities in the next subsections.

3.4.1 Pre-trial probability

Following the procedure described above, we evaluate the pre-trial probability via Monte-Carlo simulation of random data series. Let us illustrate the method with an example. We use the sampling of LSI +61°303 data in campaign II and the values of x_i randomly selected from a Poisson distribution of mean equal to the average number of events observed in 15 minutes in the real data. Using these data we calculate the power for the selected frequencies. Figure 3 shows the Rayleigh and Lomb-Scargle periodograms for such a data sample.

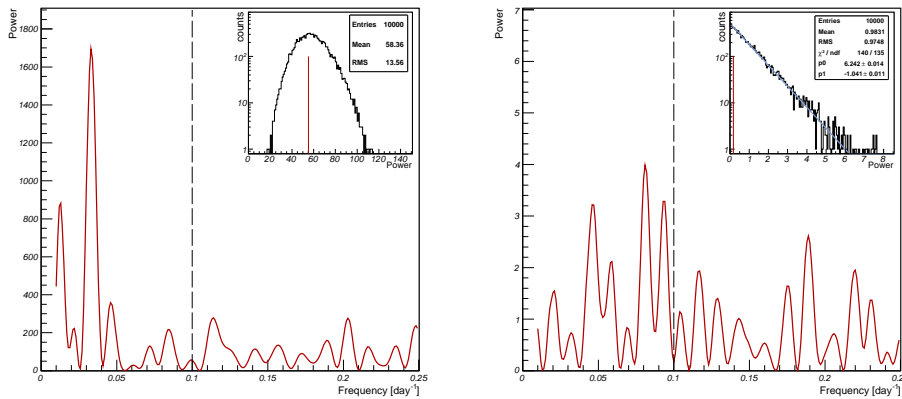


Figure 3: Rayleigh (left panel) and Lomb-Scargle (right panel) periodograms for a Monte-Carlo simulation of LSI +61°303 campaign II sampling. For every scanned frequency, the power of each test is determined. As an example, for frequency $\nu = 0.1\text{d}^{-1}$ (dashed line) we plot in the inset the distribution of the powers (PDF) of 10^4 resampled flux series. The red line in the inset marks the value of the power for the original data set (see text for details).

To estimate the probability of each power, we produce random data series by resampling the original fluxes, i.e., we keep constant the arrival times and *shuffle* the number of observed number of events. In this way, we obtain quasi-independent random data series. We produce 10^4 resampled series and calculate the periodogram for each one. For a given frequency, the probability to obtain a power value between z_0 and $z_0 + dz$ is then given by the number of simulated light curves resulting in such a power value, divided by the overall number of simulations:

$$\mathcal{P}(z_0 < P(\omega_i) < z_0 + dz) = \frac{N_{sim}(z_0 < P(\omega_i) < z_0 + dz)}{N_{sim}} \quad (12)$$

In our example, for the frequency $\nu = 0.1\text{d}^{-1}$ a power of Rayleigh test of $R(0.1\text{d}^{-1}) = 55$ is obtained. To estimate the probability of this or higher power to occur, it is compared to the distribution of the Rayleigh power (PDF) for 10^4 randomly resampled fluxes (Fig. 3 left panel, inset). The probability is the given by

$$\mathcal{P}(R(0.1\text{d}^{-1}) \geq 55) = \frac{N_{sim}(R(0.1\text{d}^{-1}) \geq 55)}{10^4} = 0.59 \quad (13)$$

The same procedure is done for the Lomb-Scargle test, where a power of $P(0.1\text{d}^{-1}) = 0.17$ is obtained, which corresponds to a probability of $\mathcal{P}(P(0.1\text{d}^{-1}) \geq 0.17) = 0.83$.

In case the power obtained for the original data series is much larger than the highest simulated power, an estimation of the probability has to be done. For the Lomb-Scargle method, as the PDF has by construction an

exponential shape, a fit is performed (see eg. inset in Fig. 3) to extrapolate up to the desired power. In figure 4 we present the pre-trial CPF of the Lomb-Scargle power, determined by Monte-Carlo simulations for the LSI +61°303 data sampling in campaign II and a frequency of $\nu = 1/26.496 \text{ day}^{-1}$. For the case of the Lomb-Scargle test, due to the fact that the periodogram is normalised to the variance σ^2 , which is estimated from the data, the probability distribution does not follow an exponential form with index -1 (classical periodogram, red line). Expression 8 (yellow line) does not reproduce either the results obtained by Monte-Carlo simulation. Therefore, as discussed in Section 3.4 we estimate the pre-trial probability (for powers above 13) using an exponential fit to the cumulative probability function obtained with the Monte-Carlo simulated (resampled) data.

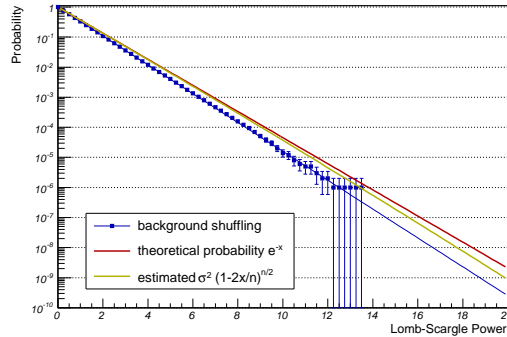


Figure 4: Pre-trial cumulative probability function of the Lomb-Scargle power determined by Monte-Carlo simulations (in blue) for LSI +61°303 campaign II sampling and frequency $\nu = 1/26.496 \text{ day}^{-1}$. The theoretical exponential density function is shown in red, whereas in yellow the expected probability density function from the normalisation of the Lomb-Scargle periodogram on the measured variance is given.

For the Rayleigh test we do not have a suitable function to describe the probability distribution, since the Rayleigh power is distributed as χ^2 with 2 degrees of freedom only if the sampling data set is uniformly distributed. In fig 5 we see as an example the power distribution of Monte-Carlo simulations of LSI +61°303 campaign II sampling, for two frequencies $\nu = 0.038 \text{d}^{-1}$ (upper panel) and $\nu = 0.060 \text{d}^{-1}$ (lower panel). A Gaussian function does not fit well. The CPF of the pre-trial probability of the Rayleigh power for those two example frequencies are also shown (right panels). The probability distributions do not follow the integral of a Gaussian distribution (*erfc* or complementary error function). We conclude that the value and distribution of the Rayleigh power changes with the frequency we study. Then if the obtained power for a given frequency is higher than the maximum simulated power, we use the RMS of the distribution to estimate the pre-trial probability. This will work in much of the cases, but will over estimate the probability as higher the power is. Nevertheless we will apply the Rayleigh test as a crosscheck with the Lomb-Scargle method, although we will draw the conclusions exclusively using the Lomb-Scargle test.

3.4.2 Post-trial probability

To obtain an appropriate post-trial probability we first construct an empirical CPF as described above, and fit this distribution with the false alarm function of choice. To exemplify it we use the second LSI +61°303 campaign sampling (as in Sec. 3.4.1). For each Monte-Carlo data series we construct the Lomb-Scargle periodogram and use the maximum obtained power at any of the scanned frequencies to build the corresponding PDF and CPF, shown in Fig. 6. For instance, by producing 10^4 resampled time series, we reach a highest Lomb-Scargle power just above 13. An exponential fit is performed for powers above 6, and the result is used to estimate the chance probability for powers above 13.

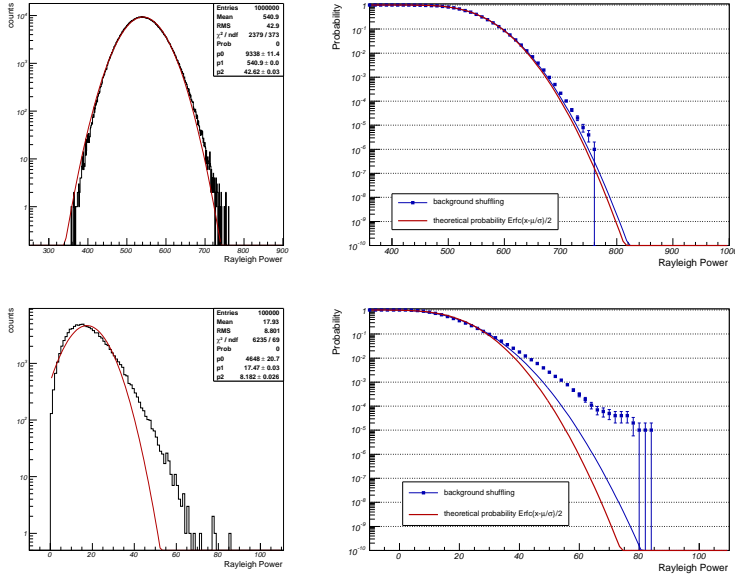


Figure 5: Example of two Rayleigh power distributions (left) and cumulative functions of the pre-trial probability (right) computed using Monte-Carlo simulations with LSI +61°303 campaign II sampling, for frequencies $\nu = 0.038 \text{d}^{-1}$ (upper panels) and $\nu = 0.060 \text{d}^{-1}$ (lower panels). As the power distributions are not symmetric they do not fit well to Gaussian functions. The red line corresponds to the complementary error function (from the integral of the Gaussian distribution) while the blue line is a fit to the data using the error function form.

As a consistency check, we have also produced the CPF by resampling of the following data series (all corresponding to campaign II sampling): the original LSI +61°303 data, the LSI +61°303 data after subtraction of the orbital period sinusoid, and an OFF sample obtained simultaneously with the LSI +61°303 data. In all those cases we obtained compatible CPFs, showing that this procedure to compute the post-trial probability only depends on the data sampling.

The post-trial PDF and CDF using the Lomb-Scargle test for the LSI +61°303 campaigns I, II and I+II samplings are shown in Fig. 7. Exponential fits to the CPFs will be used to compute the post-trial probability from the data periodograms (see Sec. 5.1).

However this method of calculating the chance probability is not feasible for the Rayleigh test in unevenly sampled data. This is due to the fact that the pre-trial probability density function strongly depends on the sampling and the tested frequency and it makes no sense to tabulate the higher Rayleigh power, since it is not the most probable. Nevertheless we calculate the Rayleigh (pre-trial) periodograms and used them for comparison and cross check of the Lomb-Scargle method.

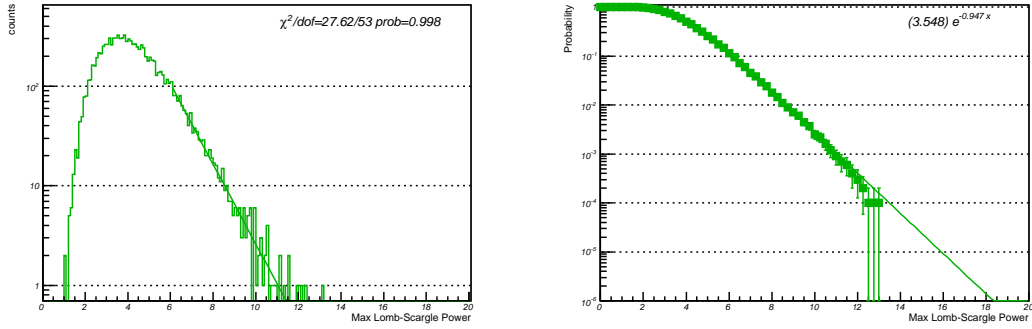


Figure 6: Distribution of the highest Lomb-Scargle power in the periodogram (left) and cumulative probability distribution (right) computed using Monte-Carlo simulations of LSI +61°303 campaign II sampling. The parameter of the exponential fit performed (in the right part of the distribution) is given in the inset.

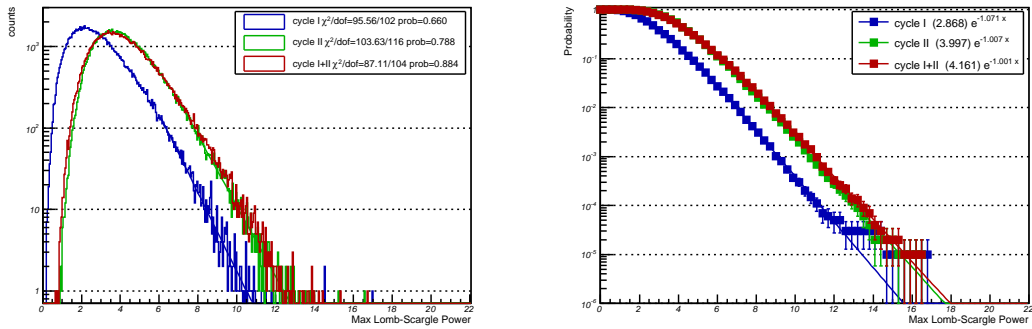


Figure 7: Unnormalized probability density functions (PDFs) of the highest Lomb-Scargle power in the periodogram (left) and corresponding cumulative probability functions (CPFs) (right) determined by random resampling of LSI +61°303 data in campaign I (in blue), II (in green) and I+II (in red). The parameters of the exponential fits performed (in the right part of the distributions) are given in the inset.

4 Technical considerations

4.1 Unphysical peaks in the periodogram

The fact that the telescope detection efficiency might show periodicities (e.g. periodic changes of zenith angle), could cause non-physical peaks in the periodogram. In order to evaluate and correct for this effect, we construct the periodogram using the OFF sample obtained simultaneously with the LSI +61°303 data. This is treated in different ways for campaigns I and II:

- For **campaign I** the data are taken in ON/OFF mode, so we use a higher hadronness cut to select a simultaneous background. As for ON data the hadronness cut is $h < 0.1$, for OFF we use ² $0.3 < h < 0.5$.
- For **campaign II**, as the data are taken in wobble mode, we use the signal candidates recorded by the anti-source positions for constructing the Lomb-Scargle periodogram.

The periodograms for campaigns I, II and I+II using the OFF samples are shown in Figs. 8, 9 and 10 (upper panels) respectively. Significant peaks (probability $< 10^{-4}$) appear for some frequencies such as: 0.016 and 0.028 day⁻¹ for the first campaign and $\nu = 0.03, 0.04$ and 0.63 day⁻¹ for the second.

To remove those unphysical peaks from the periodogram, we perform the statistical tests using the *equalised* quantity $\hat{x}_i = k_i * x_i$, where x_i are the number of γ -candidates: N_{ON} (for the Rayleigh test) or excess events N_{ex} (for the Lomb-Scargle test) reaching the telescope at time t_i ; and the equalisation weights k_i are defined as

$$k_i = \langle N_{bg} \rangle / N_{bg\ i} \quad (14)$$

for $i = 1, \dots, n$, where $N_{bg\ i}$ is the number of events detected at time t_i in the background region and $\langle N_{bg} \rangle$ their mean value.

To make this equalisation as smooth as possible, we would like to have large statistics in the background estimation N_{bg} . Therefore, for the evaluation of the weights in *campaign II*, we use the mean background from the 3 OFF regions and apply a softer hadronness cut. For the signal extraction, we use a hadronness cut with γ -ray efficiency 0.8. We see in Fig. 11 that the background events obtained with efficiencies 0.8 and 0.95 are well correlated. Then one may use the second, softer cut in order to have more statistics for the background estimation in the equalisation. For *campaign I*, we used a different hadronness cut $0.5 < h < 0.6$ of simultaneous data, where the signal contribution is not expected³, and use it for the equalisation.

In order to check if the equalisation method eliminates the spurious frequencies due to the detection efficiency, we build the periodogram for the OFF samples, but using the equalized quantities \hat{x}_i . The results for the Lomb-Scargle and Rayleigh tests for the different campaigns are shown in Fig. 8, 9 and 10 (lower panels). For campaign II we perform this test over three different samples corresponding to the three independent OFF wobble regions. In each case, the weights k_i are computed using the remaining two OFF samples. We obtain no significant probability peaks in any of the samples for any of the tested frequencies and those obtained from the non-equalised data are removed.

The fact that we use this equalization method prevents us to use the γ -ray flux as physical magnitude in the statistical test. For calculating the flux from the number of excess, we use (apart from the observation time) the effective area, which is obtained from Monte-Carlo. And Monte-Carlo takes into account known variations (as zenith angle) while the equalization procedure considers those and any other variations (such as weather conditions).

²We tested with Crab of the same period that this cut does not contain significant signal

³Also tested with the Crab data sample.

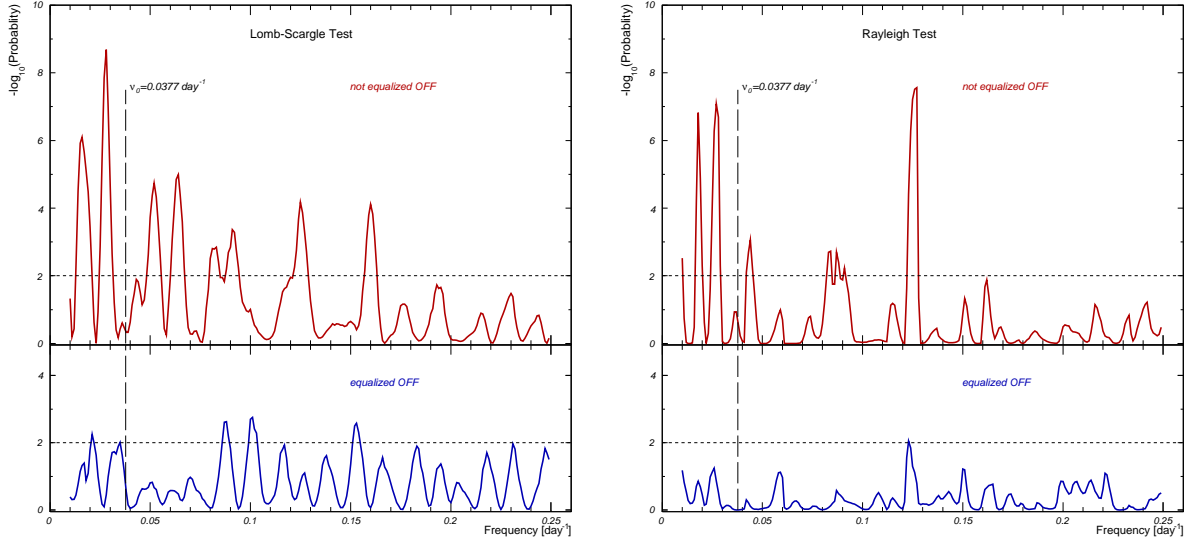


Figure 8: Periodogram obtained with the Lomb-Scargle (left) and Rayleigh (right) tests for the OFF region in campaign I: The upper (lower) panel shows the probabilities for the OFF region without (with) equalisation. The vertical dashed line marks the LSI +61°303 orbital frequency. The horizontal dotted line marks the level of probability $< 10^{-2}$.

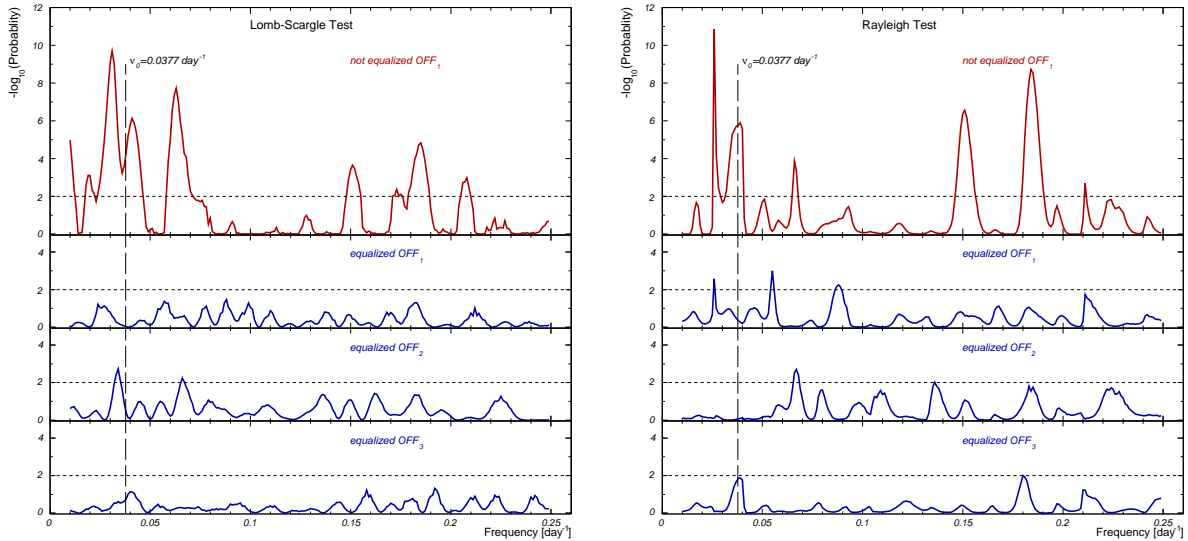


Figure 9: Periodogram obtained with the Lomb-Scargle (left) and Rayleigh (right) tests for the OFF data in campaign II: Upper panels show the probabilities for one anti-source region without equalisation applied; second, third and last panels show the probabilities for each one of the three independent OFF regions, equalised using the data from the remaining two. The vertical dashed line marks the LSI +61°303 orbital frequency. The horizontal dotted line marks the level of probability $< 10^{-2}$.

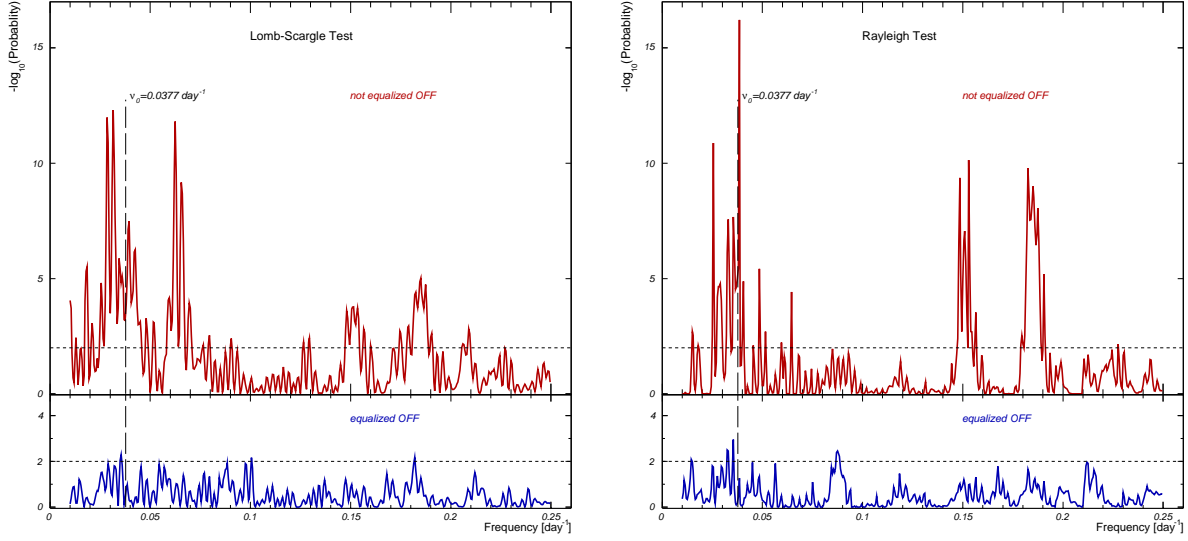


Figure 10: Lomb-Scargle (left) and Rayleigh (right) periodograms for the OFF region in campaign I+II: The upper (lower) panels show the probabilities for the OFF region without (with) equalisation. The vertical dashed line marks the LSI +61°303 orbital frequency. The horizontal dotted line marks the level of probability $< 10^{-2}$.

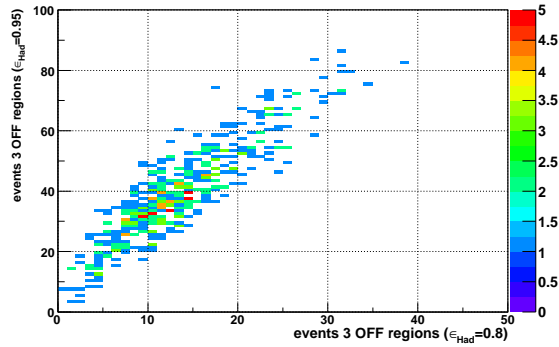


Figure 11: Distribution of OFF events together in the 3 OFF regions of LSI +61°303 campaign II, for hadronness cut with γ -ray efficiency 0.8 versus distribution with efficiency cut 0.95.

4.2 Merging data form different observational campaigns

We want to perform the statistical tests using campaigns I, II and I+II both together, in order to increase the number of measurements and the total elapsed time (between the first and last observation).

Due to the difference in time between the two observational campaigns (6 months) and the change in the observation mode, we expect the telescope sensitivity to be different. Moreover, the analyses themselves are different: the γ -ray rate (recorded from Crab Nebula samples contemporaneous to each campaign) is different. For those reasons, we define a new quantity, comparable between both campaigns, to be able to perform the statistical tests.

In the case of Lomb-Scargle method, we use for the individual campaign test the number of excess N_{ex} . The phaseogram with LSI +61°303 data of each individual campaign is shown in Fig. 12 (left panel). To scale N_{ex} to the same level we use the relation between two Crab data analyses, contemporaneous with each of the LSI +61°303 campaigns. In all analyses we used the same energy threshold of 400 GeV. For campaign I we used 212 minutes of Crab data taken in October and November 2005. With an analysis completely analogue to the one performed over LSI +61°303 data in campaign I we obtain an excess rate of $R_{CI} \simeq 287 \pm 10 N_{ex}/h$. For campaign II, 116 minutes of Crab data in September 2006 were analysed in the same way as LSI +61°303 campaign II, with an excess rate of $R_{CII} \simeq 156 \pm 9 N_{ex}/h$. Thus the scale factor between LSI +61°303 data campaigns is $S_{ex} = R_{CII}/R_{CI} = 0.55$, and the phaseogram with the scaled number of excess is shown in Fig. 12 (right panel).

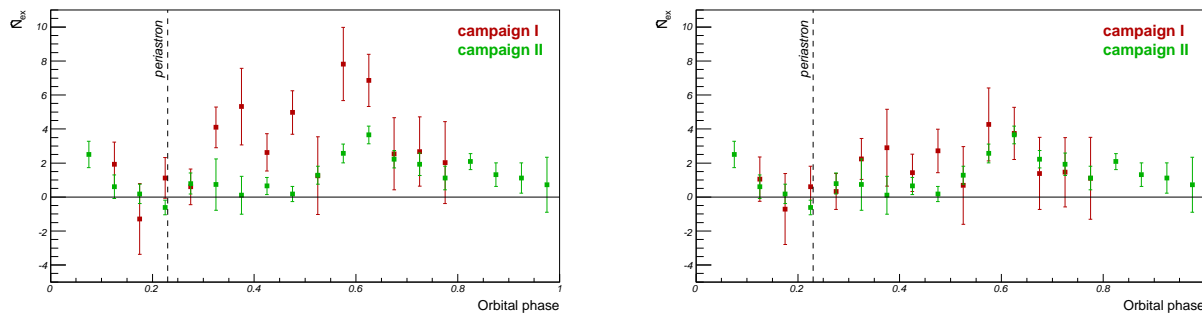


Figure 12: Number of equalized γ -excess for first (red) and second (green) campaigns versus LSI +61°303 phase (folded with the orbital frequency). Each analysis campaign has a different N_{ex} level (left panel), which is scaled by a factor 0.55 obtained from the analysis of Crab Nebula samples, to obtain a comparable base line (right panel).

To scale the OFF data (that we use for crosscheck, as e.g. in Sec. 4.1) we proceed in the same way: by comparing the Crab analyses. As the normalization factors in each campaign are different, we use the relation between the background rate in the Crab campaigns which are 1.29 and 0.39 N_{ex}/min , respectively. This yields a scale factor of $S_{OFF} = 0.30$. The phaseogram for N_{OFF} with and without applying the scale factor are presented in Fig. 14.

For the Rayleigh test, we use the N_{ON} as physical variable, the direct comparison with Crab is not feasible. As an approximation, we used the same scale factor as in the OFF data set S_{OFF} . The phaseograms with and without applying the scale factors are shown in Fig. 13.

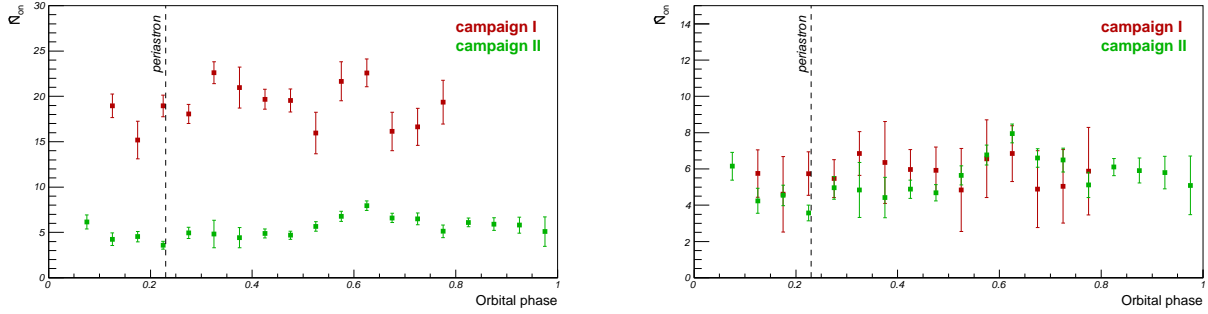


Figure 13: Number of equalized N_{ON} for first (red) and second (green) campaigns versus LSI +61°303 phase (folded with the orbital frequency). Each analysis campaign has a different level (left panel), which is scaled by a factor to obtain a comparable base line (right panel). See text for details.

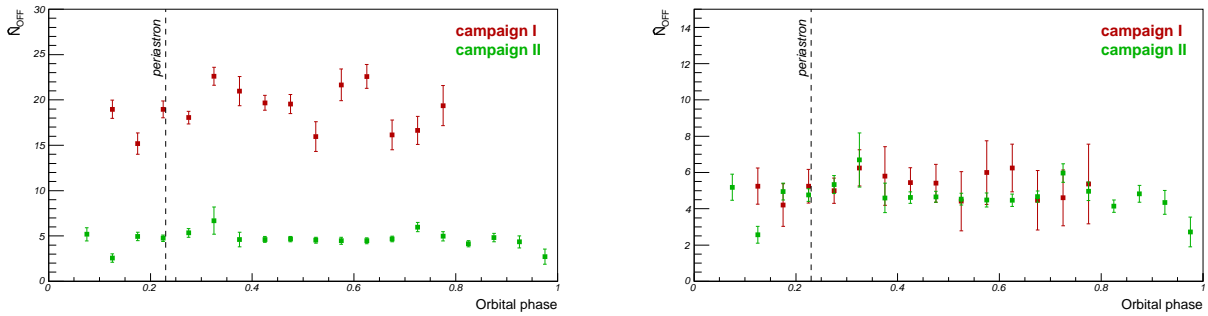


Figure 14: Number of equalized N_{OFF} for first (red) and second (green) campaigns versus LSI +61°303 phase (folded with the orbital frequency). Each analysis campaign has a different level (left panel), which is scaled by a factor to obtain a comparable base line (right panel). See text for details.

5 Results

5.1 Periodograms over LSI +61°303 data

We apply the Rayleigh and Lomb-Scargle statistical tests to the **LSI +61°303 data campaign I**. The results are presented in Fig. 15. A maximum peak in the periodogram probability is seen for frequency $\nu = 0.038\text{d}^{-1}$ and $\nu = 0.035\text{d}^{-1}$ with the Lomb-Scargle and Rayleigh tests, respectively. The pre-trial chance probability is about 10^{-5} . Using the CPF shown in Fig. 7, we compute the corresponding post-trial probability, which results to be 2.0×10^{-4} .

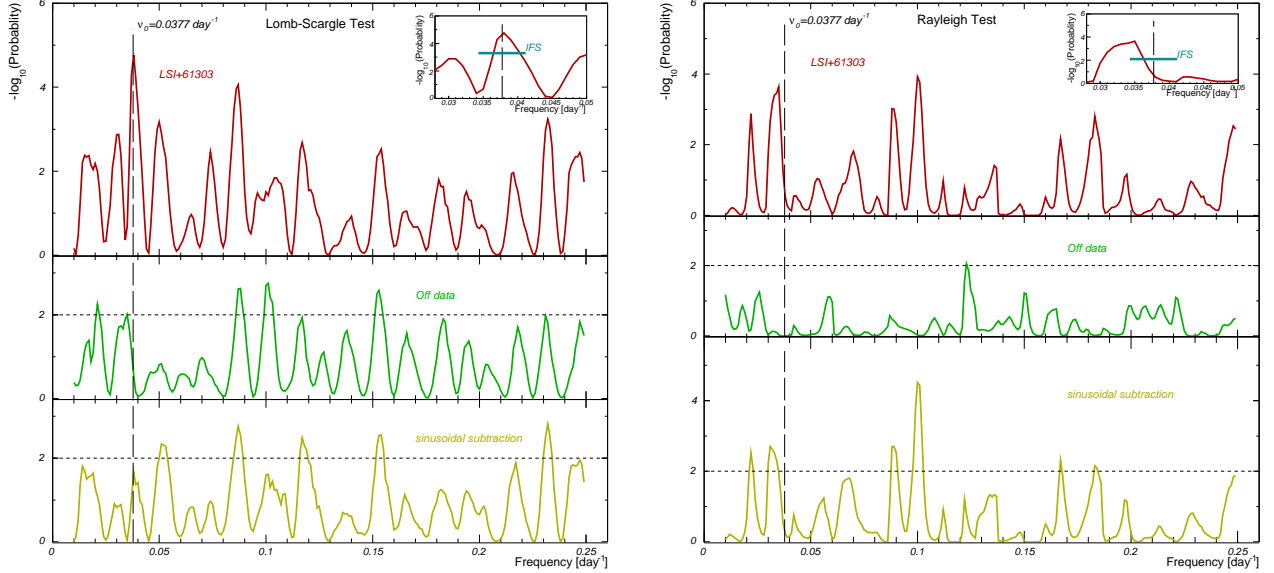


Figure 15: Pre-trial periodogram for Lomb-Scargle (left) and Rayleigh (right) test over the LSI +61°303 data in campaign I (upper panel) and OFF data (middle panel). In the lower panel we present the probabilities for the data after subtraction of a purely sinusoidal signal at the orbital period. The vertical dotted line corresponds to the orbital frequency.

We apply the test to the **campaign II data** and obtain the periodogram shown in Fig. 16. In this case a maximum peak in the Lomb-Scargle periodogram probability is clearly seen for frequency $\nu = 0.038\text{d}^{-1}$, for which we obtain a Lomb-Scargle power of ~ 17 . It is highly significant with a pre-trial chance probability of about 10^{-8} . The post-trial chance probability of the peak is found to be lower than 0.8×10^{-7} . For the Rayleigh statistical test, the maximum peak is seen at $\nu = 0.040\text{d}^{-1}$, with a power of 223, which corresponds to a pre-trial probability of $\sim 10^{-10}$.

The fact that the power obtained in campaign I is lower than the one obtained in campaign II is due to the lower observation time (54 hours compared to the 112h in campaign II) and because the orbital coverage is lower: in the 6 observed periods there are no data taken below phase 0.1 neither above phase 0.8. While in campaign II we observed 4 periods but a better coverage was achieved.

We **combined campaigns I and II data**, which allows us to scan more frequencies, because the elapsed time between first and last measurement is 442 days. The results are shown in Fig. 17. A peak at frequency $\nu = 0.038\text{d}^{-1}$ is seen with a Lomb-Scargle power of ~ 22 , which gives a pre-trial chance probability about 10^{-12} . The corresponding post-trial probability is 1.3×10^{-9} . Similar behaviour is observed for the Rayleigh test with a maximum in $\nu = 0.038$

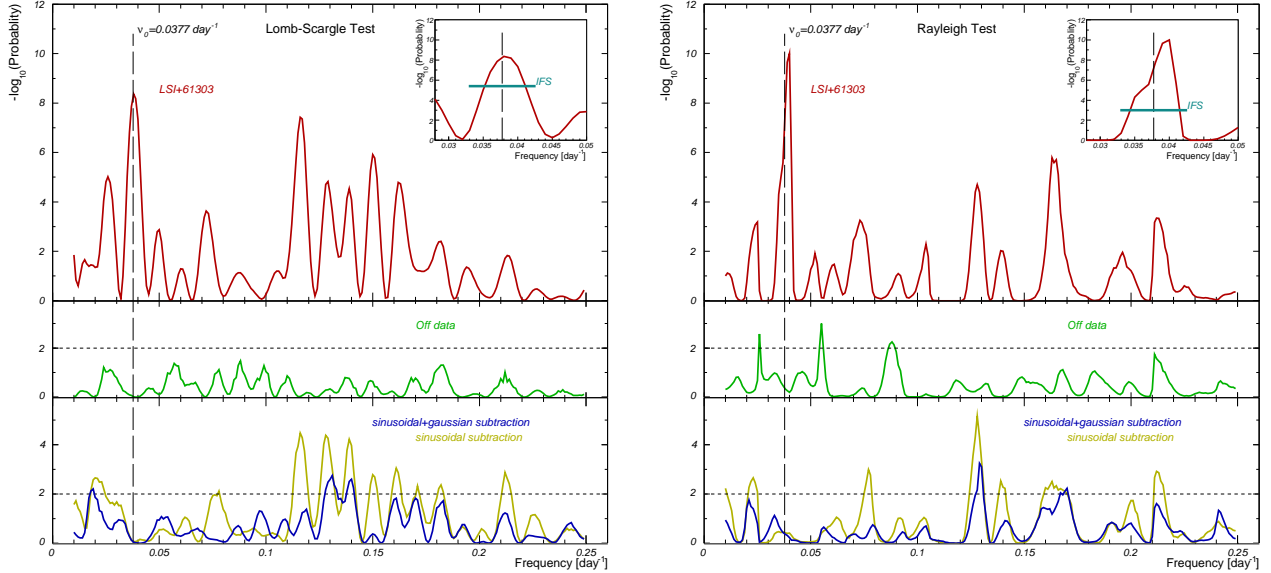


Figure 16: Pre-trial periodogram for Lomb-Scargle (left) and Rayleigh (right) test over the LSI +61°303 data campaign II (upper panel) and OFF data (middle panel). In the lower panel we present the probabilities for the data after subtraction of a purely sinusoidal signal at the orbital period of the system (yellow line) and after subtraction of a sinusoidal plus a Gaussian peak (blue line). Vertical dotted line corresponds to a frequency of 0.037 day^{-1} .

which has a probability of $\sim 10^{-12}$.

Also less prominent but significant peaks are detected for other frequencies. For instance, in the Lomb-Scargle periodogram, the frequencies 0.041 , 0.115 and 0.150 d^{-1} have pre-trial probabilities of about 10^{-8} , 10^{-10} and 10^{-8} , respectively. All those peaks are related to the signal, as they do not show up in the OFF data (Fig. 17, middle panel). These are beat periods of the orbital period with various gaps present in the LSI +61°303 data-set, that is, rational fractions of beat periods added to the orbital period.

The data have been folded with the orbital frequency ($\nu = 0.037 \text{ d}^{-1}$) for campaign I, II and I+II. The results are presented in fig 18. A sinusoidal fit is performed in each case, and the obtained parameters are given in the inset.

If we subtract the sinusoidal signal from the fit to the data and perform the statistical tests, we obtain the periodogram probabilities shown in Figs. 15, 16 and 17 (lower panels, yellow line) for LSI +61°303 data campaign I, II and I+II respectively. The peak corresponding to the orbital frequency has been removed in all cases as expected. With subtracting the orbital period we also remove or reduce some satellite peaks. But the fact that those other peaks do not achieve a level consistent with the background test indicates that the signal in LSI +61°303 data is not purely sinusoidal.

We also subtract a sinusoidal plus a Gaussian signal contribution, fitted to campaign II and campaign I+II data ⁴ (fig 18, green dotted lines). The corresponding periodograms are presented in Fig. 16 and Fig. 17 (lower panels, blue lines). The orbital frequency peak has been removed and the rest of the periodogram peaks are much more reduced than in the purely sinusoidal subtraction, being compatible with the background periodogram.

To crosscheck these results, we apply the Rayleigh and Lomb-Scargle methods over a simulated sample containing a sinusoidal signal similar to that found in the data. For each arrival time t_i , taken from the real data, we simulate

⁴For campaign I alone, this function is difficult to fit (see folded phaseogram in Fig. 18) due to the uncovered phases and so we did not try this test on these data.

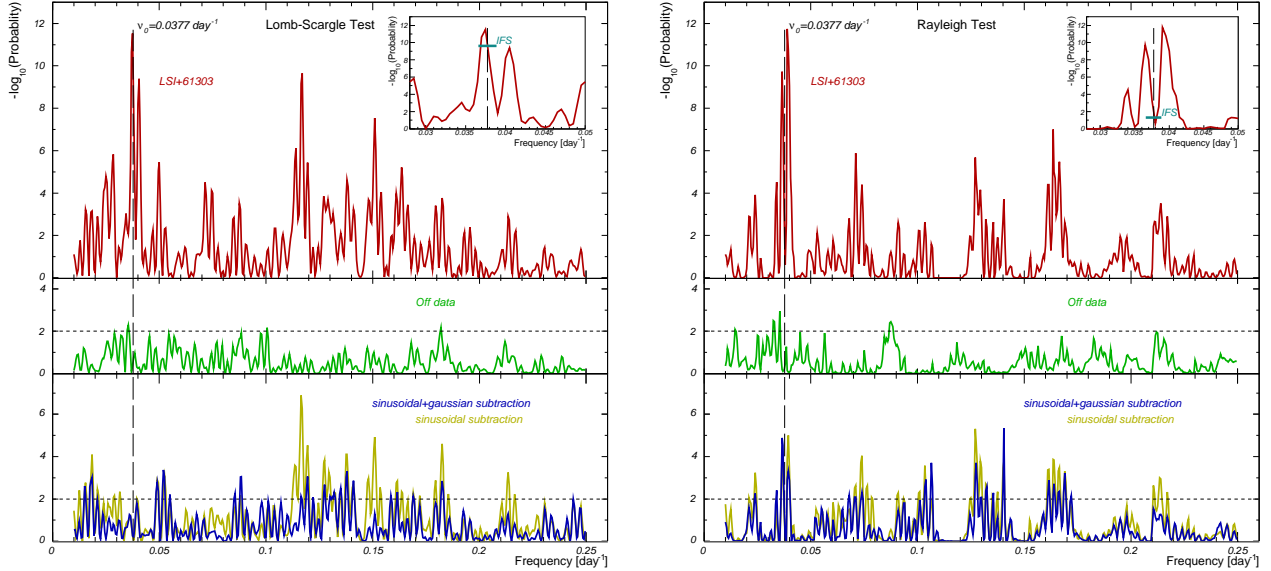


Figure 17: Pre-trial periodogram for Lomb-Scargle (left) and Rayleigh (right) tests over the LSI +61°303 combined campaign I+II data (upper panel) and OFF data (middle panel). In the lower panel we present the probabilities for the data after subtraction of a purely sinusoidal signal at the orbital period (yellow line) and a sinusoidal plus a Gaussian wave form (blue line). The dotted vertical line corresponds to a frequency of 0.037 day^{-1} (period of 26.496 days).

a signal as a random Gaussian with mean $B + A \cdot \sin(2\pi(\phi_i + \phi_0))$ where A , B and ϕ_0 are taken from the sinusoidal fits to the data folded with the orbital period; the width σ of the Gaussian function is taken from the data spread in the phaseogram. We obtain the periodogram shown in Figure 19, using time bins of 15 minutes. We detect a signal of about 10^{-18} chance probability for $\nu = 0.037 \text{ d}^{-1}$ for Lomb-Scargle test and campaign I data. The same procedure is done for campaign II and we obtain a probability of 10^{-39} for the same frequency. For campaign I+II a peak with probability 10^{-45} is detected for frequency $\nu = 0.0375 \text{ d}^{-1}$.

So far, we have scanned the periodograms up to frequency 0.25 d^{-1} , which includes the orbital period of interest, but due to the long elapsed observation time, we are able to search for higher frequencies (see Sec. 3.3). To search for possible features in the high frequency region, we perform an extended Lomb-Scargle test for LSI +61°303 campaign II data as shown in Fig. 20. Apart from the already discussed periodogram peaks around the orbital period, we see significant signals (probability lower than 10^{-4}) in frequencies 1.04 (period about 23 h), 2.04, 3.08, 4.8 and 5.08 d^{-1} . From the OFF periodogram (Fig. 20 middle panel) we see that those peaks are related intrinsically to the LSI +61°303 data, as they do not appear in the simultaneous background. However, if we subtract a sinusoidal or a Gaussian plus a sinusoidal function to the data, the peaks (together with the orbital peak) disappear or reduce up to the level of the background probabilities. We conclude that those peaks are due to aliasing effects. In fact, the highest peak at about one day we already expected from the windowing function (see Sec. 3.3) because the measurements were done mostly in consecutive nights.

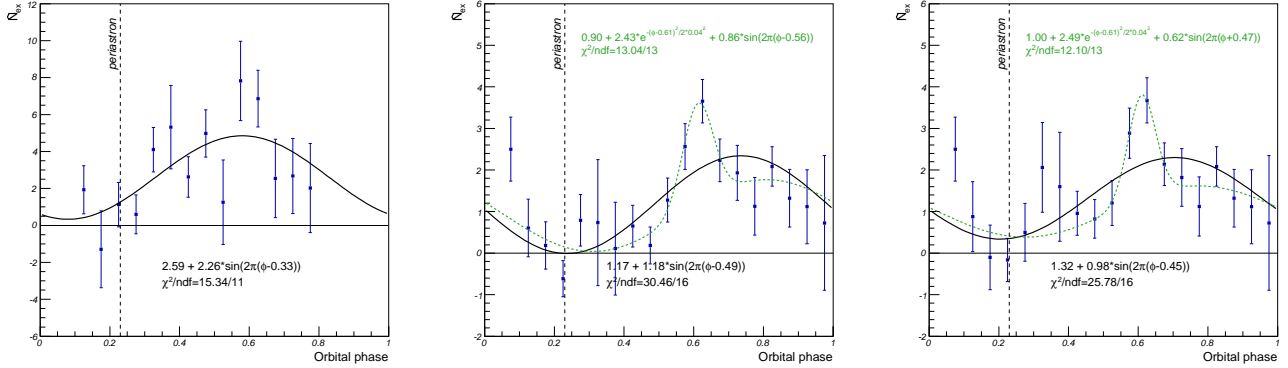


Figure 18: LSI +61°303 (equalized) number of γ -candidates folded with the frequency $\nu = 1/26.496\text{day}^{-1}$. From left to right we present data for campaigns I, II and I+II. Black curves are fits to a sinusoidal signal (fit parameters are given in the insets). For campaign II and I+II, there is also the possibility to investigate other wave forms, and we fitted a sinusoidal signal plus a Gaussian component (green dashed lines), which adjusts better to the data ($\chi^2/\text{dof}= 11.53/13$ for campaign I+II). Vertical dotted line indicates the periastron passage.

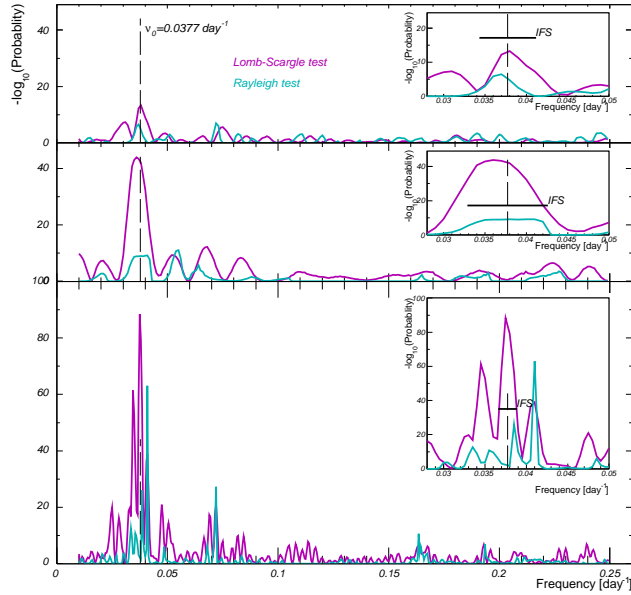


Figure 19: Pre-trial periodogram for a simulated sinusoidal signal using the Rayleigh (blue) and Lomb-Scargle (pink) tests for campaigns I (upper panel), II (middle panel) and I+II (lower panel).

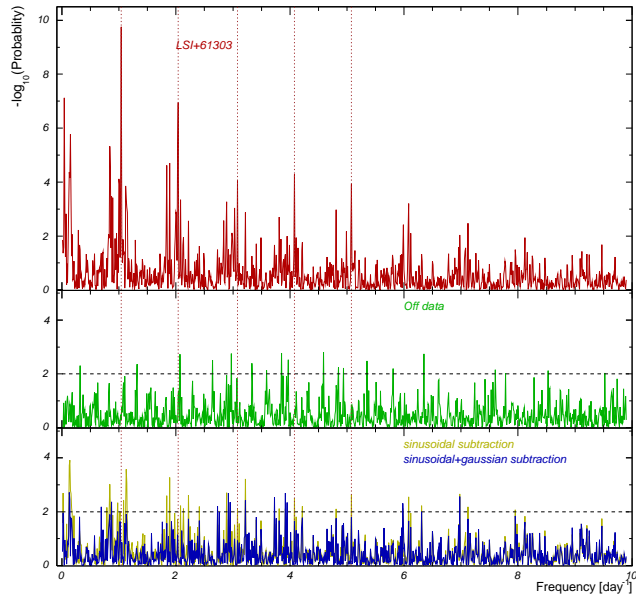


Figure 20: Extended (scanned up to frequency 10 d^{-1}) periodogram for Lomb-Scargle test over the LSI +61°303 data campaign II (upper panel) and OFF data (middle panel). In the lower panel we present the periodogram for the data after subtraction of a purely sinusoidal signal at the orbital period of the system (yellow line) and after subtraction of a sinusoidal plus a Gaussian peak (blue line). Vertical dotted lines mark significant peaks in the LSI +61°303 periodogram which disappear or reduce in the all other periodograms.

5.2 Analysis for different time bins

All previous results are obtained using bins of 15 minutes. In this section we study the effect of the bin size (Δt) on our results.

From inspection of Eq. 6 it becomes evident that:

- the Lomb-Scargle power increases with the number of points: for a sinusoidal signal in a data set with n points, $(x_i - \bar{x}) \propto \sigma \cos \omega t$ or $(x_i - \bar{x}) \propto \sigma \sin \omega t$ and then

$$P(\omega) \propto \frac{1}{2\sigma_X^2} \left[\frac{[\sum_{i=1}^n \sigma \cos \omega t_i \cos \omega t_i]^2}{\sum_{i=1}^n \cos^2 \omega t_i} + \frac{[\sum_{i=1}^n \sigma \sin \omega t_i \sin \omega t_i]^2}{\sum_{i=1}^n \sin^2 \omega t_i} \right], \quad (15)$$

therefore $P(\omega) \propto n$. And so the probability will increase with the number of points in the data set, for the same number of scanned frequencies (same number of trials). Averaging the data increases the effective sampling interval Δt , thus decreasing the Nyquist frequency. If we scan the averaged data set at a lower number of frequencies, the post-trial probability will also decrease. The fact that the post-trial probability increases with the number of scanned frequencies is the *statistical penalty* that we must pay for inspecting a large number of frequencies[2].

- Successive sub-divisions of a data sample produce progressively less effect on the CDF, until it eventually converges to a limiting CDF beyond which no further division of the sample changes the result. The original time domain data contain a finite amount of information. There is therefore a limit to how much information they can be forced to yield.
- A binning of half a day or day-by-day is not appropriate because different days have different observation times and hence different errors. But as the statistical tests used here do not treat with errors, all points are weighted the same. In case of fixed-time bins, all points have similar weight in the periodogram. This effect becomes even worst since the LSI +61°303 orbit is not uniformly covered: we observed more days and for longer times in phases with expected higher flux, about $\phi \sim 0.6$, and hence their relative weight in the periodogram is very much reduced by taking a fixed number of data points per night.

The periodograms obtained in campaign II using bins of 7.5, 15, 30 and 60 minutes, half nights and night-by-night bins are shown in Fig. 21. We see that the significance of the peak around frequency 0.0377 decreases for wider bins, except between 7.5 and 15 minute bins, where the saturation limit is reached. The amplitude of the folded data with the orbital frequency (see inset in Fig. 21) scales approximately proportionally with the size binning. The main difference when combining data for widening bins is the loss of statistics. The number of data points decreases from 419 points in 15 minutes bins to 51 points in night-by-night bins.

The second peak seen in Fig. 21 at frequency $\sim 0.12\text{d}^{-1}$ (about 8 days) is a beat period of the 0.037d^{-1} peak. We saw that it decreases when subtracting a sinusoidal signal and vanishes for a sinusoidal plus Gaussian signal (Fig 16 lower panel).

To confirm these results we have generated Monte-Carlo data series with the sampling and sinusoidal signals corresponding to the different time binnings. The Lomb-Scargle power for frequency 0.037d^{-1} is reduced as the bin width increases as seen in Fig. 22. The power obtained for the same frequency with LSI +61°303 data is also shown for comparison (Fig. 22, blue points).

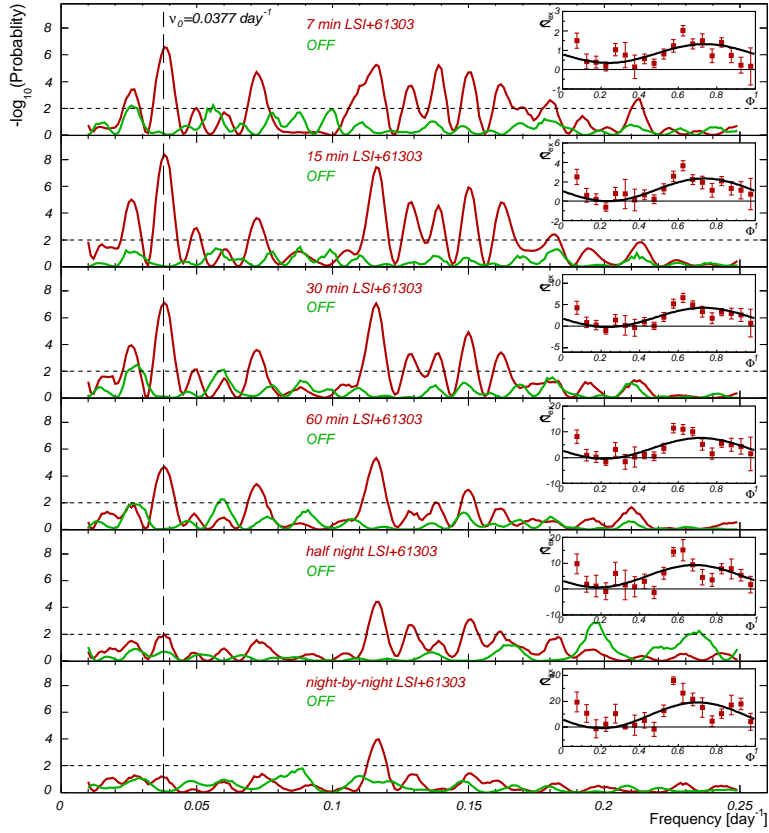


Figure 21: From top to bottom: Periodogram for Lomb-Scargle test over the LSI +61°303 campaign II data using 7.5, 15, 30 and 60 min, half-night and night-by-night bins. Red curves are for LSI +61°303 data while green curves are for OFF data. In the inset, the phase folded data for the orbital frequency is fitted with a sinusoidal function.

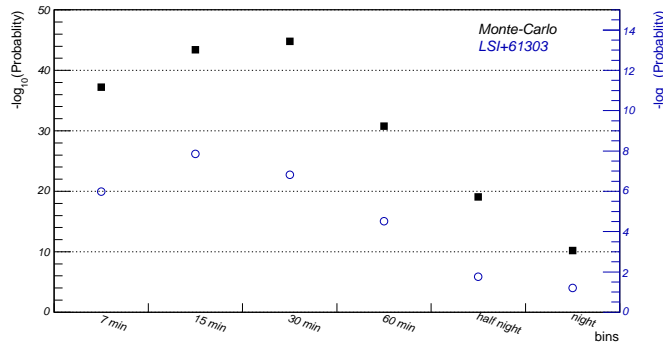


Figure 22: Pre-trial probability for LSI +61°303 campaign II and frequency 0.037d^{-1} obtained using Lomb-Scargle test with different time-bins for a simulated sinusoidal signal (in black) and the real data (in blue, right axis).

5.3 Peak frequency and error estimation

In case of evenly sampled data, the distance between independent frequencies (see Sec. 3.3) is the Independent Fourier Spacing (IFS): for instance in LSI +61°303 campaign II the elapsed time is $T \simeq 100$ days, and the number of points $n \simeq 500$ points, for 15 minutes time bins; in this case we may scan the natural frequencies (Eq. 9) from $\nu_1 = 1/100 = 0.01\text{d}^{-1}$ to $\nu_{250} = 250/100 = 2.5\text{d}^{-1}$. The step between those natural frequencies is the IFS $1/T \simeq 1/100 = 0.01\text{d}^{-1}$. However, the position of the peak in a periodogram can be estimated with better accuracy than this value.

An accurate peak frequency determination is done by scanning more frequencies (increasing the oversampling factor) around the frequency which has maximum probability in the periodogram. The power values around the most probable frequency for each campaign are shown in Fig. 23 and the frequency values are summarised in table 2.

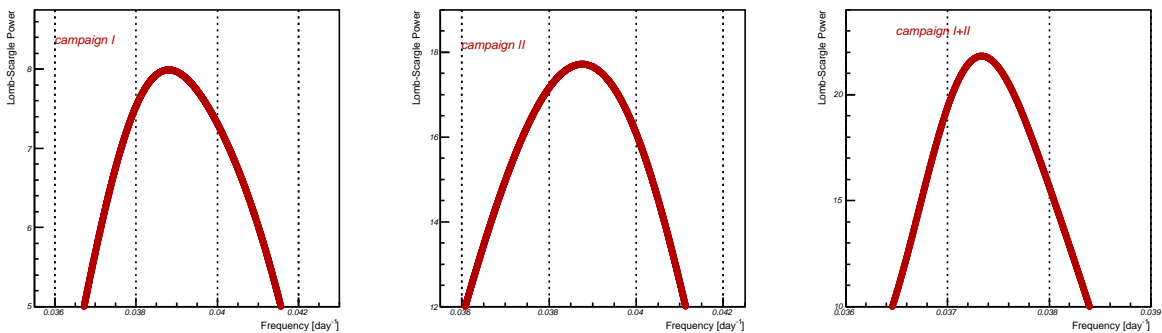


Figure 23: Lomb-Scargle powers around the most probable frequencies in the periodograms for LSI +61°303 campaigns I, II and I+II (from left to right).

In case the sample is unevenly spaced, while the statistical properties of the periodograms have received much attention, the frequency error estimation is rarely discussed in the literature [13]. We will discuss below two different approaches.

Sometimes, an astrophysical quantity is not an obvious function of the observed data, thus, the regular error propagation formula cannot be applied to estimate the error of the corresponding quantity. This is the case of the signal frequency derived from power spectrum, which is a function of the data, but the exactly form is hard to be obtained. We therefore applied a Monte Carlo simulation to evaluate the error in the frequency estimation, as we did for the false alarm probability (see Sec. 3.4).

One possible approach to the error estimation is the following: we simulate light curves where the number of γ -ray candidates are selected randomly from a Poisson distribution of mean equal to the actually measured number of events arriving at every given time.

The periodogram is calculated for 10^3 of those randomly generated series, and the distribution of the resulting peak power frequencies are shown in Fig. 24. The region around the orbital frequency is fitted with a Gaussian function. The other peaks can be attributed to the aliasing effect and are of no interest for this study.

For campaign I+II we obtain an error of 0.00013d^{-1} which corresponds for the orbital period to an error in the period of 0.09 days. The frequency value is calculated with enough accuracy by increasing the oversampling in the LSI +61°303 Lomb-Scargle periodogram. The frequency and period with their errors obtained for the different campaigns are given in table 2.

Under the assumption of a purely sinusoidal signal, we can estimated the frequency error from Monte-Carlo simulated time series containing a sinusoid, with the same characteristics (amplitude, phase origin and base line) as the obtained with the fitted data (see Fig. 18). With 10^3 of these data series we construct the distribution of the

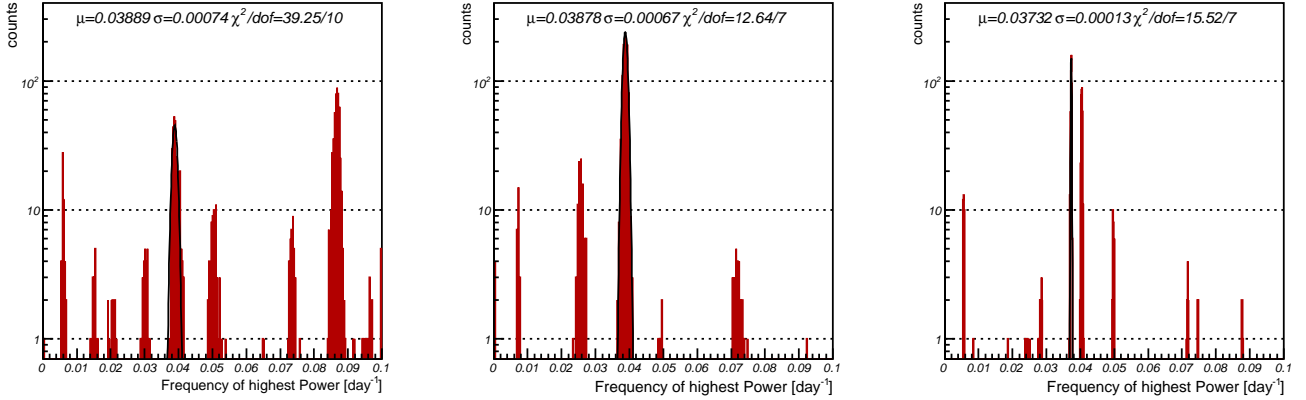


Figure 24: Distribution of frequencies with the highest Lomb-Scargle power determined by letting the data points in the LSI +61°303 light curve vary according to a Poissonian distribution. From left to right: campaigns I, II and I+II.

highest power in the periodogram, shown in Fig. 25. The frequency and period together with the estimated errors, for each campaign, are shown in table 2. In the campaign I+II, we obtain an error of 0.00005d^{-1} which corresponds to an error in the period of 0.03 days.

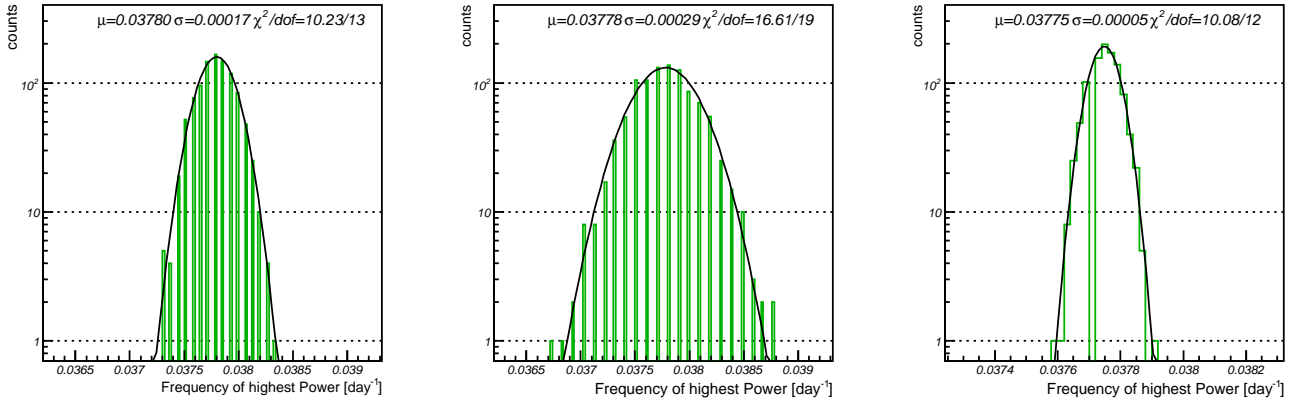


Figure 25: Distribution of frequencies with the highest Lomb-Scargle power determined by Monte-Carlo simulated time series for campaigns I (left), II (middle) and I+II (right panel).

6 Conclusions

A search for periodicity over LSI +61°303 TeV data in campaign I, II and I+II has been carried out using the Lomb-Scargle and Rayleigh statistical tests. The associated (post-trial) chance probability has been calculated by Monte-Carlo simulations on each specific unevenly sampling for the Lomb-Scargle method.

Campaign	Lomb-Scargle				IFS (d ⁻¹)
	Poisson Errors		Sinusoidal with Gaussian Errors		
	ν (d ⁻¹)	P (d)	ν (d ⁻¹)	P (d)	
I	0.0388 ± 0.0007	25.8 ± 0.5	0.03880 ± 0.00017	25.77 ± 0.12	2.0 × 10 ⁻⁴
II	0.0388 ± 0.0007	25.8 ± 0.4	0.0388 ± 0.0003	25.8 ± 0.2	0.8 × 10 ⁻⁷
I+II	0.03734 ± 0.00013	26.78 ± 0.09	0.03734 ± 0.00005	26.78 ± 0.03	1.3 × 10 ⁻⁹

Table 2: For each observational campaign we present the frequency ν and period P with their error obtained with two different methods and the Lomb-Scargle periodograms: Poissonian propagation of errors and a sinusoidal with Gaussian errors. The IFS value is also given. The post-trial chance probability of the frequency peak is quoted for each campaign.

The periodograms for each campaign show up peaks around the orbital frequency $\nu = 1/26.496\text{d}^{-1}$. The peak is purely associated with the LSI +61°303 data, as it does not appear for the simultaneous OFF data periodogram (see Fig. 17). Some other peaks that appear in the periodogram are beat periods of the orbital period with various gaps present in the data-set. This is seen when subtracting a purely sinusoidal signal to the data, and performing the same statistical test. In this case, the orbital frequency peak is removed as expected, but also those satellite peaks are removed or reduced. If instead we subtract a sinusoidal plus a Gaussian signal contribution (as see in the periodogram Fig. 18) the satellite peaks are much more reduced, being compatible with the background periodogram level.

As expected the most accurate frequency value is obtained after merging the data from both campaigns, which yields a period value of **26.78±0.09** days with a post-trial probability of **10⁻⁹**. The frequency error has been estimated as a propagation of the Poissonian measurement errors. If a sinusoidal signal is assumed, the error is much reduced up to **26.78±0.03** days. But the signal subtractions we already performed over the periodograms suggested a non purely sinusoidal form of the signal, thus we take the confident value obtained without any signal forma assumption.

References

- [1] Lomb, N. R. Least - squares frequency analysis of unequally spaced data. *Astrophys. Space Sci.*, 39:447–462, 1976.
- [2] Scargle, J. D. Studies in astronomical time series analysis. 2. Statistical aspects of spectral analysis of unevenly spaced data. *Astrophys. J.*, 263:835–853, 1982.
- [3] Mardia, K. V. *Statistics of Directional Data*. Academic Press, New York, 1972.
- [4] Gregory, P. C. and Taylor, A. R. *Nature*, 272:704–706, 1978.
- [5] Casares, J., Ribas, I., Paredes, J. M., Marti, J., and Allende Prieto, C. Orbital Parameters of the Microquasar LSI +61 303. *Mon. Not. Roy. Astron. Soc.*, 360:1091–1104, 2005.
- [6] Gregory, P. C. *Astrophys. J.*, 575:427–434, 2002.
- [7] Paredes, J. M. and Figueras, F. Detection of optical variability of LSI + 61 303. *Astron. Astrophys.*, 154:L30–L32, 1986.
- [8] Taylor, A. R. et al. *Astron. Astrophys.*, 305:817–824, 1996.

- [9] Tavani, M. et al. *Astrophys. J.*, 648:L89–L91, 1998.
- [10] Fomin, V. P. et al. New methods of atmospheric Cherenkov imaging for gamma-ray astronomy. 1: The False source method. *Astropart. Phys.*, 2:137–150, 1994.
- [11] Schwarzenberg-Czerny, A. The distribution of empirical periodograms: Lomb-Scargle and PDM spectra. *Mon. Not. Roy. Astron. Soc.*, 301:831–840, December 1998.
- [12] Frescura, F. A. M. and Engelbrecht, C. A. and Frank, B. S. Significance Tests for Periodogram Peaks. 2007.
- [13] Akerlof, C. et al. Application of cubic splines to the spectral analysis of unequally spaced data. *Astrophys. J.*, 436:787–794, December 1994.